

**SUPPLEMENTARY MATERIAL****jp0682816***Journal of Physical Chemistry A, Received December 1, 2006***Supporting Information.**

Note, references are numbered as in the manuscript.

**S1. Details of MQC MD calculations.**

The electronic structure calculations described in this paper were performed on clusters of water molecules extracted from a 100-ps adiabatic MQC MD trajectory with a time step of 1 fs. In this trajectory, the water molecules moved classically according to the velocity Verlet algorithm<sup>22</sup> and the single excess quantum mechanical electron was confined to its adiabatic ground state. The 200 water molecules occupied a cubic 18.17 Å x 18.17 Å x 18.17 Å simulation cell and interacted with each other through SPCf (flexible simple-point charge) potentials.<sup>23</sup> The excess electron interacted with the water molecules through a pairwise-additive pseudopotential,  $V_p$ ,<sup>24</sup> and at every time step the ground-state wave function,  $\psi$ , of the electron was calculated on a 16 x 16 x 16 cubic grid using an iterative-and-block-Lanczos algorithm.<sup>25</sup> The force exerted by the electron on the water molecules was of the Hellmann-Feynman form,  $F_i = -\langle \psi | \nabla_i V_p | \psi \rangle$ , where  $F_i$  is the force on atom  $i$  and  $\nabla_i$  denotes a gradient with respect to the spatial coordinates of atom  $i$ . The average temperature of the system was 296 K with root-mean-square fluctuations of 8 K.

Figure 1S(a) exhibits the distribution function  $g(r_{XH})$  for the  $r_{XH}$  distances, which has its first maximum at 2.26 Å. This pair distribution function is similar to the one obtained in identical MQC MD simulations by Schwartz and Rossky using a much larger sample of  $e_{hyd}^-$  configurations.<sup>9</sup> In Figure 1S(b), we plot a histogram for the smallest of the  $X-O-H_{in}$  angles for water molecules in the first solvation shell. The most probable value of this angle is 12-14° and the largest such angle is still less than 60°: the OH bonds in the first solvation shell clearly point preferentially towards X, consistent with previous conclusions from the literature.<sup>8,9</sup>

**S2. Further information on the CIS methods.**

It is interesting to note that when we were exploring the effect of different basis sets and cluster sizes on the calculated absorption spectrum of  $e_{hyd}^-$  with CIS we found that a spectrum that more closely resembles the experimental one (including the characteristic "tail" in the blue) was obtained in a CIS( $N=20$ )/6-31+G\*\* calculation that included only one complete solvation shell of water molecules and no "ghost atom" (Figure 6S(a)). Furthermore, almost perfect agreement with the experiment was obtained when in the latter calculation the matrix of point charges was removed (Figure 6S(b)). This illustrates the great sensitivity of the calculated CIS spectra to the details of cluster embedding and the presence of a "ghost atom." This sensitivity, in turn, is explained by the large spatial extent of the ground and especially the excited states and the difficulty in representing the parts of the electron's ground and excited-state wavefunctions far from

atom centers which in turn leads us to believe the agreement with experiment for the single solvation shell model was fortuitous.

Isovalue surfaces for the three lowest excited states calculated according to section 3.2 are shown in Figure 9S, panels (c) to (e). Also shown are the HOMO and HOMO-1 for the ground state wavefunction (Figure 9S, panels (a) and (b), respectively). Comparing to the isodensity surfaces of the DFT orbitals (plotted at a similar contour level), shown in Figures 3, 7S, and 8S(b), we see qualitatively the same behavior: the ground state excess electron is mainly localized in the cavity with some mixing into the first shell water *p*-like orbitals; the HOMO-1 is made up of  $1b_1$  orbitals on nearby waters; and the first three excited states are *p*-like, with polarization in roughly orthogonal directions, and extend beyond the cavity having considerable overlap with the first shell waters.

### S3. The unoccupied DFT Kohn-Sham orbitals.

In Figure 7S, we show isodensity contour plots for the DFT KS HOMO, HOMO-1, LUMO, LUMO+1, and LUMO+2 for one of the snapshots. Overall, we see a similar picture to that observed in our CIS calculations of the  $e_{hyd}^-$  (section 3.2 and Figure 9S). That said, the familiar dumbbell shape of the '*p*-orbital' is not readily recognizable in the three lower unoccupied states, although these states do exhibit *p*-like polarization, each orthogonal to the others (Figures 7S); only a fraction of the total '*p*-state' density (ca. 20%, Figure 10S(a)) is contained inside the cavity. By contrast, 60% of the density of the ground '*s*-state' is confined inside the cavity and 80% is confined within the first solvation shell (Figure 4b). The *p*-character of these electronic states is achieved partially through the polarization of the frontal *O*  $2p$  orbitals in the OH groups forming the cavity (Figure 8S): the phase of the electron in these orbitals on one side of the cavity assumes a positive sign, while the phase of the electron in the *O*  $2p$  orbitals straight across the cavity in the direction of the transition dipole moment assumes a negative sign. We also see both positive and negative excess electron density in the interstitial cavities between the water molecules of the first and the second solvation shells. The ensemble average '*p*-like states' extend further out of the cavity than the '*s*-like' state: the corresponding gyration ellipsoid is 1.8 Å x 2.2 Å x 3.3 Å (Figure 10S(b)), which is nearly twice the size of the gyration ellipsoid for the SOMO, as might be expected for a *p*-like state. The excitation thus changes the electron's radial distribution function maximum from 1.72 Å to 3.3 Å (Figures 4b and 10S(a)), with most of the electron density contained in the interstitial voids between the water molecules of the first and the second solvation shells.

Given the correspondence between the DFT and CIS excited states, we expect that the energy gap between the DFT SOMO and three LUMOs should be in the region of the maximum of the  $e_{hyd}^-$ 's absorption spectrum. To examine this, in Figure 4S(b), we plot histograms of the corresponding transition energies, which indeed show three distinctive *p*-subbands with centroids at 2.11, 2.34, and 2.55 eV; we note that these histograms are *not* identical with the spectra because we have not weighted these by their corresponding oscillator strengths. We thus confirm that the DFT unoccupied KS orbitals can be used as a qualitative model of the excited states of the  $e_{hyd}^-$ .

#### S4. Rationalizing EPR spectra for $^{17}\text{O}$ enriched samples.

For  $^{17}\text{O}$  nuclei, the second moment of the EPR spectrum is ca.  $6 \times 10^3 \text{ G}^2$ , almost all of which is due to the *isotropic* hyperfine interaction (see above). For the 37% oxygen-17 enriched sample studied by Schlick et al.,<sup>5a</sup> using eq. (B7) in ref. 1 we obtained  $M_2 \approx 2250 \text{ G}^2$  vs. the reported experimental estimate of  $134 \text{ G}^2$ . As we observed in Part 1,<sup>1</sup> *all* ab initio and DFT models of the hydrated electron tend to give such large estimates for  $M_2^O$ . We note, however, that the experimental estimate of Schlick et al.<sup>5a</sup> was compromised by their subsequent observation<sup>5b</sup> of a strong spectral overlap between one of the resonance lines of the  $\text{O}^-$  radical and the narrow EPR signal from the “electron,” which had  $\Delta B_{pp} \approx 18 \pm 1 \text{ G}$ . In alkaline glasses, the  $\text{O}^-$  anion is formed with the same yield in the same radiolytic reaction that yields the  $e_{\text{hyd}}^-$ . In  $^{16}\text{O}$  glasses, the two narrow EPR signals from  $e_{\text{hyd}}^-$  and  $\text{O}^-$  are spectrally well separated, but because the signals overlap in  $^{17}\text{O}$  enriched samples, the EPR spectrum in such enriched samples is very complex: there are 7 lines from  $^{17}\text{O}^-$  spanning 400 G with the  $g_{\parallel}$  component (Figure 1 in ref. 5b) strongly overlapping with the EPR signal from the electron. Thus, the small  $M_2$  estimate of  $134 \text{ G}^2$  given by Schlick et al., that was obtained using  $^{17}\text{O}$  enriched samples, is subject to some doubt.

To better understand the EPR spectrum of the enriched samples, in Figure 14S(b), we used our calculated hfc tensors for  $^1\text{H}$  and  $^{17}\text{O}$  nuclei to simulate the EPR spectrum of an oxygen-17 enriched sample. The EPR line decomposes into two distinct spectral contributions, a narrow one with  $\Delta B_{pp} \approx 23 \text{ G}$  and  $M_2 \approx 135 \text{ G}^2$  (in good agreement with the estimates of Schlick et al.<sup>5a</sup>) and a very broad line with  $\Delta B_{pp} \approx 89 \text{ G}$  and  $M_2 \approx 1980 \text{ G}^2$ . For a sample with 37%  $^{17}\text{O}$  enrichment, there is a ca. 10% probability that the first solvation shell would have no magnetic oxygen-17 nuclei. We assign the narrow line as arising from such isotopic configurations, so that the electron is only weakly coupled to the oxygen-17 nuclei in the second solvation shell. The isotope configurations that include at least one oxygen-17 nucleus in the first solvation shell, on the other hand, are responsible for the broad line. It is worth noting that our simulation in Figure 14S(b) neglects any differences in the paramagnetic relaxation of these two kinds of hydrated electrons. Small-amplitude movement of water molecules in the frozen samples would cause efficient spin relaxation, due both to the large hfcc's on the first-shell oxygens and the steep dependence of the isotropic hfcc on the X-O distance (Figure 12S(a)). The narrow line from the electron in the 37%  $^{17}\text{O}$  enriched sample is superimposed on a much broader signal that was attributed to one of the components of the  $^{17}\text{O}^-$  radical multiplet (that shows a complex pattern of broad lines). This narrow resonance line was recognized as the EPR signal originating from the  $e_{\text{hyd}}^-$  from the microwave power saturation behavior of the spin transition, i.e., this line was selected by its long relaxation time. Broad resonance lines that were not saturated were attributed to the  $^{17}\text{O}^-$  radical. Such a criterion for the recognition of the (tentative) EPR signal from the  $e_{\text{hyd}}^-$  discriminates against broad EPR signals with short relaxation times that are expected for trapped electrons that are strongly coupled to  $^{17}\text{O}$  in the first solvation shell.

We believe, therefore, that the EPR results of Schlick et al.<sup>5</sup> do not contradict our hybrid DFT model, as the experimental results may be accounted for by assuming that only weakly coupled electrons (for which the magnetic <sup>17</sup>O nuclei are in the second solvation shell only) are selected using the *ad hoc* criterion suggested by Schlick et al.:<sup>5b</sup> electrons that are strongly coupled to the <sup>17</sup>O nuclei in the first solvation shell relax rapidly and have broad EPR lines that are superimposed on the comparably broad lines from the <sup>17</sup>O<sup>-</sup> radical.

To conclude, fast paramagnetic relaxation and extreme broadening of EPR lines from the hydrated electrons involving <sup>17</sup>O nuclei in the first solvation shell bias the observation towards the isotope configurations in which no <sup>17</sup>O nuclei are present in this shell. With these assumptions, we are able to quantitatively account for the linewidths of the EPR spectra for trapped  $e_{hyd}^-$ ,<sup>4,5</sup> both with and without <sup>17</sup>O enrichment.

## Figure Captions (Supplement)

### Figure 1S

(a) *Solid black lines, to the left:* Pair distribution  $g(r)$  of the  $r_{XH}$  distances between the center of mass of the electron (MQC MD calculation, 200 snapshot average) and the protons. *Red curve, to the right:* the same distribution after weighting by a factor  $4\pi r^2$ . Both of these distributions have the first maxima at 2.26 Å. (b) *Solid black lines:* The distribution  $\alpha_{XOH}$  defined as the smallest of the two XOH angles for the protons in the water molecules in the first solvation shell for which  $r_{XH} < 3$  Å. The *red curve* is the power-exponential fit to  $\alpha^m e^{-\alpha/\alpha_0}$ , where  $m=1.63$  and  $\alpha_0=7^\circ$ . The most probable X-O-H angle is ca. 12-14° and all of these angles are within a 60° cone, i.e. the solvating OH groups tend to point towards X.

### Figure 2S

(a,b) Two sequential snapshots of hydrated electron,  $e_{hyd}^-$  (the time interval  $\Delta t = 100$  fs). Isodensity maps of singly occupied molecular orbitals are shown for (from top to bottom)  $\pm 0.02$ ,  $\pm 0.04$ , and  $\pm 0.05 a_0^{-3}$ , calculated using the DFT/6-311++G\*\* model with  $r_{cut}=4.75$  Å. The cross at the cavity center indicates the center of mass X of the electron in the MQC MD model; pink is for positive, violet is for negative part of the SOMO wavefunction for the embedded water cluster anions ( $r_{cut} = 4.75$  Å; (a)  $n=21$ ,  $\phi_{2p}^O \approx 0.16$ ; (b)  $n=22$ ,  $\phi_{2p}^O \approx 0.18$ ; in both cases the electron is sixfold coordinated).

### Figure 3S

Enlarged, color version of Figure 6 in the text. (a) KS density of states function, DOS (the occupancy number is shown) for 'hydrated electron' ( $r_{cut}=4.75$  Å, which corresponds to the first two solvation shells). The arrows indicate the position of (i) HOMO (SOMO) and (ii) the three lowest unoccupied states (shown separately in Figure 3S). The red curve is for occupied  $\alpha$ -MO's (the same spin orientation as that for the unpaired electron), the green curve is for unoccupied  $\alpha$ -MO's; the scattered black dots are the DOS for  $\beta$ -MO's; the yellow line is the total DOS. (b) The same as (a), for  $\alpha$ -MO's in the embedded neutral water clusters ( $r_{cut}=3.5$  Å; dashed blue curve), and the first solvation of the hydrated electron ( $r_{cut}=3$  Å clusters): the violet curve is for the water anion, the yellow curve is for a neutral water cluster (of the same geometry) with a negative point charge placed at the electron's center of mass (X).

### Figure 4S

(a) KS density of states (DOS) function for HOMO (SOMO) and the three lowest unoccupied molecular orbitals (MO's): LUMO, LUMO+1, and LUMO+2 (see the legend in the plot), with the maxima at -1.8, 0.34, 0.56, and 0.77 eV, respectively, calculated

using the DFT/6-311++G\*\* model with  $r_{cut}=4.75$  Å. The typical isodensity maps of such states are shown in Figures 7S and 8S. These states are related to the  $s$ - and  $p$ -like states of  $e_{hyd}^-$  in one-electron models. (b) The histograms of the corresponding transition energies (that exhibit the maxima at 2.05, 2.27, and 2.5 eV, respectively).

### Figure 5S

(a) Absorption spectra of the  $e_{hyd}^-$  calculated using three CIS models for the same 100 fs x 1000 snapshot MQC MD trajectory. Models (i) and (ii) are CIS( $N=10$ )/6-31+G\* calculations for  $r_{cut}$  of (i) 3 Å and (ii) 4.75 Å, with a ghost atom at the electron's center of mass. Model (iii) is a CIS( $N=20$ )/6-31++G\*\* calculation for cutoff radius of 3 Å without the ghost atom. The dashed trace is experimental spectrum. This plot illustrates the sensitivity of the calculated CIS spectra to the details of cluster embedding and the basis. (b) The correlation of the transition energies  $E_{0k}$  for the lowest ( $k = 1,2,3$ ) three electronically excited states of  $e_{hyd}^-$  and corresponding transition moments  $\mu_{0k}$ , for the three lowest (' $p$ -') subbands (model (iii))

### Figure 6S

The same as Figure 7, for CIS model (iii) instead of model (ii) (see the caption to Figure 5S), (a,b) with and (c,d) without the embedding matrix of SPCf charges. In panels (b) and (d), we plotted the fits of our calculated CIS spectrum to a Gaussian-Lorentzian function that is typically used to approximate the experimental spectra of solvated electron:<sup>32</sup> for  $\Delta E = E - E_m > 0$ , the amplitude is proportional to  $(1 + [\Delta E/W_L]^2)^{-1}$ ; for  $\Delta E < 0$ , it is proportional to  $\exp(-[\Delta E/W_G]^2)$ . For the  $e_{hyd}^-$  in water at 300 K,  $W_G \approx 0.42$  eV and  $W_L \approx 0.49$  eV.<sup>33</sup> The optimum fit to our CIS spectrum in panel (b) gives  $E_m \approx 2.04$  eV and 0.63 and 0.49 eV, respectively, for these two parameters.

### Figure 7S

Typical isodensity surfaces for (a) HOMO (SOMO), (b) HOMO-1, (c) LUMO, (d) LUMO+1, and (e) LUMO+2 orbitals (all for the same snapshot of the 'hydrated electron') calculated using the DFT/6-311++G\*\* model with  $r_{cut}=4.75$  Å. Positive density is shown in pink, negative is shown in violet. The isodensity levels are  $\pm 0.03 a_0^{-3}$ . The directions of the transition dipole moments are indicated by arrows. These three directions are orthogonal for these lowest unoccupied states.

### Figure 8S

Isodensity surface for the LUMO at four isodensity levels: (a)  $\pm 0.01$ , (b)  $\pm 0.02$ , (c)  $\pm 0.03$ , and (d)  $\pm 0.04 a_0^{-3}$  calculated using the DFT/6-311++G\*\* model with  $r_{cut}=4.75$  Å.

### Figure 9S

The same as Figure 7S but from a CIS( $N=10$ )/6-31+G\* calculation on a different snapshot. (a) HOMO (SOMO), (b) HOMO-1, (c) LUMO, (d) LUMO+1, (e) LUMO+2 orbitals. Positive density is shown in pink, negative is shown in violet. The isodensity levels are  $\pm 0.025 a_0^{-3}$ . Figures (c)-(e) are generated from orbitals calculated with eq. (11). The directions of the transition dipole moments are indicated by arrows. These three directions are orthogonal for these lowest unoccupied states.

### Figure 10S

(a) As Figure 4b, for the lowest three unoccupied KS orbitals (' $p$ -states'). The black curve to the left is the angle averaged density  $4\pi r^2 \rho(r)$  given by eq. (5) (the thick grey curve to the right is the integral of this radial density). The dashed black curve is the least squares fit to  $\Psi_p(r) \propto r \exp(-r/\lambda)$  for  $\lambda \approx 1.8 \text{ \AA}$ . (b) The distributions of semiaxes of the gyration tensor for the three ' $p$ -states' (see the legend). The mean meridional eccentricity of these three excited states is ca. 0.79, which is close to the theoretical 0.75 for a  $p$ -orbital, and the mean radius of gyration is  $r_g \approx 4.33 \text{ \AA}$  (vs.  $2.75 \text{ \AA}$  for the HOMO).

### Figure 11S

Histograms of (a) spin and (b) charge densities for embedded water anion clusters, as determined using Mulliken population analysis, for (i)  $H_{in}$  atoms that have  $r_{XH} < 3 \text{ \AA}$ , (ii) O atoms in the first solvation shell, (iii)  $H_{in}$  atoms that have  $r_{XH} > 3 \text{ \AA}$ , and (iv) O atoms in the second solvation shell (see section 2 for the definition of these atom groupings). The spin density in the latter oxygen atoms is close to zero. In panel (b), solid black lines give the charge densities on oxygen (on the left) and hydrogen (on the right) for embedded (neutral) water monomers. Both the unpaired electron and the excess charge density are limited primarily to the first solvation shell.

### Figure 12S

The correlation plots of (a) isotropic hfcc on oxygen-17 vs. the X-O distance and (b) the  $zz$  (long axis) component of the anisotropic hfc tensor for protons (the experimental estimate is 7 G) vs. the same value estimated in point-dipole approximation (see Appendix B in ref. 1 for more detail). In (a), "inside" (open red circles) and "outside" (open blue squares) correspond to oxygen nuclei in the first and the second solvation shell respectively (see the legend and section 2). The dots are values for every  $^{17}\text{O}$  nucleus in a cluster, symbols are cluster average values for every snapshot. The grey curve in (a) is the fit to  $\propto \exp(-2r/\lambda_o)$ ; the optimum length parameter  $\lambda_o \approx 1.59 \text{ \AA}$  of this fit is close to the localization radius ( $\lambda \approx 1.67 \text{ \AA}$ ) of the electron in the SOMO, see Figure 4b.

### Figure 13S

Histograms of (a)  $^{17}\text{O}$  and (b)  $^1\text{H}$  contributions to the second moments  $M_2^O$  and  $M_2^H$ , respectively, to the EPR spectrum of ('trapped') hydrated electron (the mean values are given in Table 1). The same calculation as in Figure 8.

**Figure 14S**

Simulated EPR spectra of  $e_{hyd}^-$  in (a)  $H_2^{16}O$  and (b) 1.7:1  $H_2^{16}O:H_2^{17}O$  solid water (the composition of the sample in the experiment of Schlick et al.<sup>5</sup>). See Appendix B of ref. 1 for the details of the simulation procedure. The red dots are the histogram of resonance offsets  $\Delta B$ . The red curve is the convolution of this histogram with the Gaussian line broadening function (the broadening was assumed to be 1 G for (a) and 5 G for (b)); the green curves (to the right) are the first derivatives of the convoluted EPR spectra. The black curve in (a) is a Gaussian fit to the convoluted spectrum. The peak-to-peak line width  $\Delta B_{pp}$  (the field interval between the points of maximum slope in the EPR spectrum or the maxima in its first derivative) is 9.1 G vs. the experimental  $9.5 \pm 0.5$  G (Astashkin et al.<sup>6</sup>). The black curve in (b) is a fit using two Gaussian functions; their derivatives (pink curve (i) and turquoise curve (ii)) and the sum (yellow curve) are shown in the same plot. The broad component (i) with  $\Delta B_{pp} \approx 89$  G (corresponding to  $M_2 \approx 1980$  G<sup>2</sup>) is from isotope configurations corresponding to at least one oxygen-17 in the first solvation shell of  $e_{hyd}^-$ . The narrow component (ii) with  $\Delta B_{pp} \approx 23$  G (vs. experimental  $18 \pm 1$  G)<sup>5a</sup> and  $M_2 \approx 135$  G<sup>2</sup> (vs. experimental  $155$  G<sup>2</sup>)<sup>5a</sup> is from isotope configurations in which the electron coupled only to  $^{17}O$  nuclei in the second solvation shell. The calculation does not take into account paramagnetic relaxation in the electron strongly coupled to  $^{17}O$  nuclei in the first solvation shell.

**Figure 15S.**

Vibrational density of states, VDOS (the density of normal modes) calculated for embedded anion and neutral (Figure 11) SPCf water clusters (solid red and dashed blue lines, respectively). Only the low energy range ( $< 2000$  cm<sup>-1</sup>) is shown. Observe the red shift of the 1000 cm<sup>-1</sup> (libration) and 1700 cm<sup>-1</sup> (H-O-H bend) bands and the prominent 100 cm<sup>-1</sup> (3 THz) band corresponding to vibrations of the water molecules relative to each other. This low-frequency band is barely seen in the IR spectra shown in Figures 11 and 12, as such vibrations have very low oscillator strength.

Figure 1S; Shkrob et al.

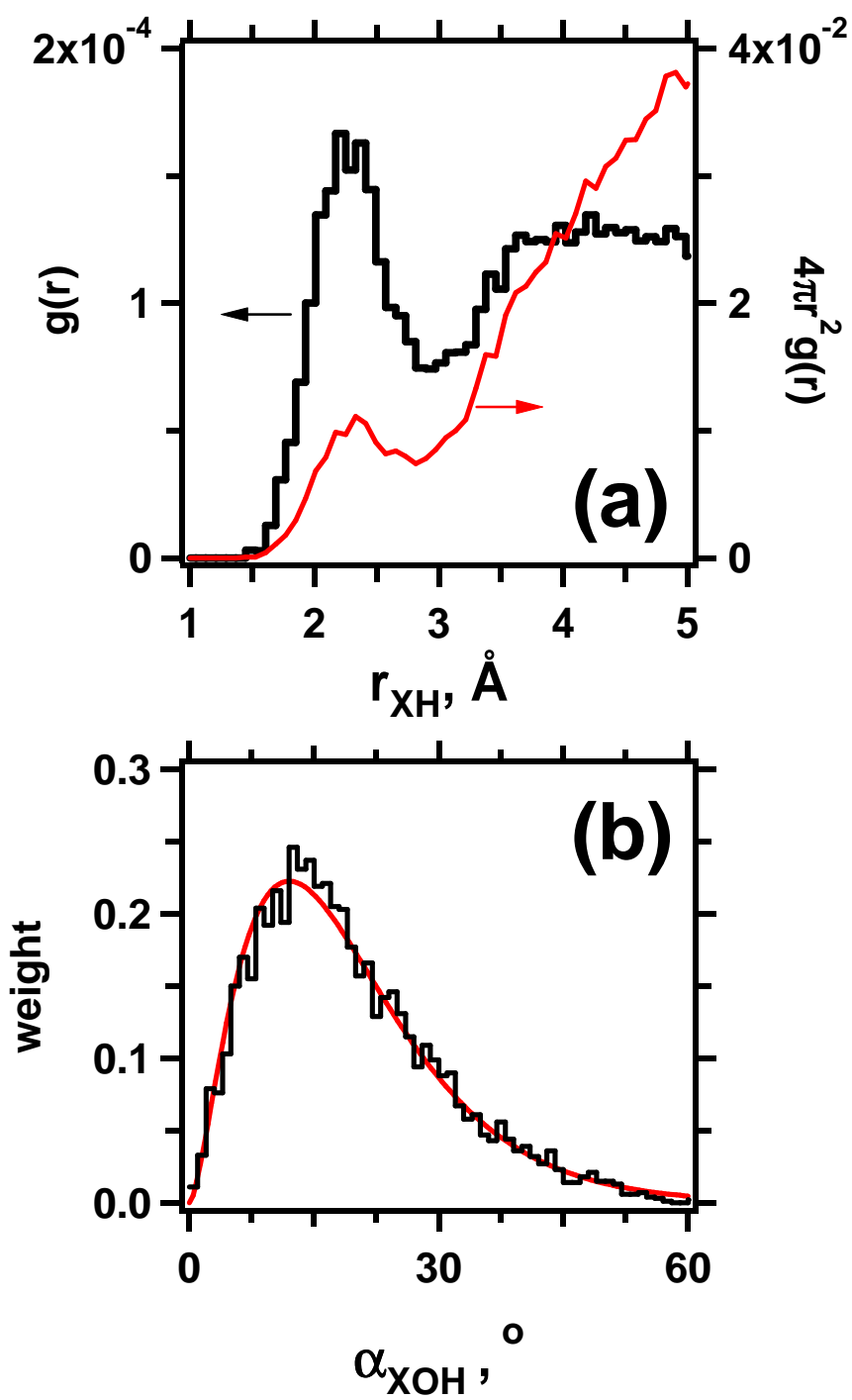


Figure 2S; Shkrob et al.

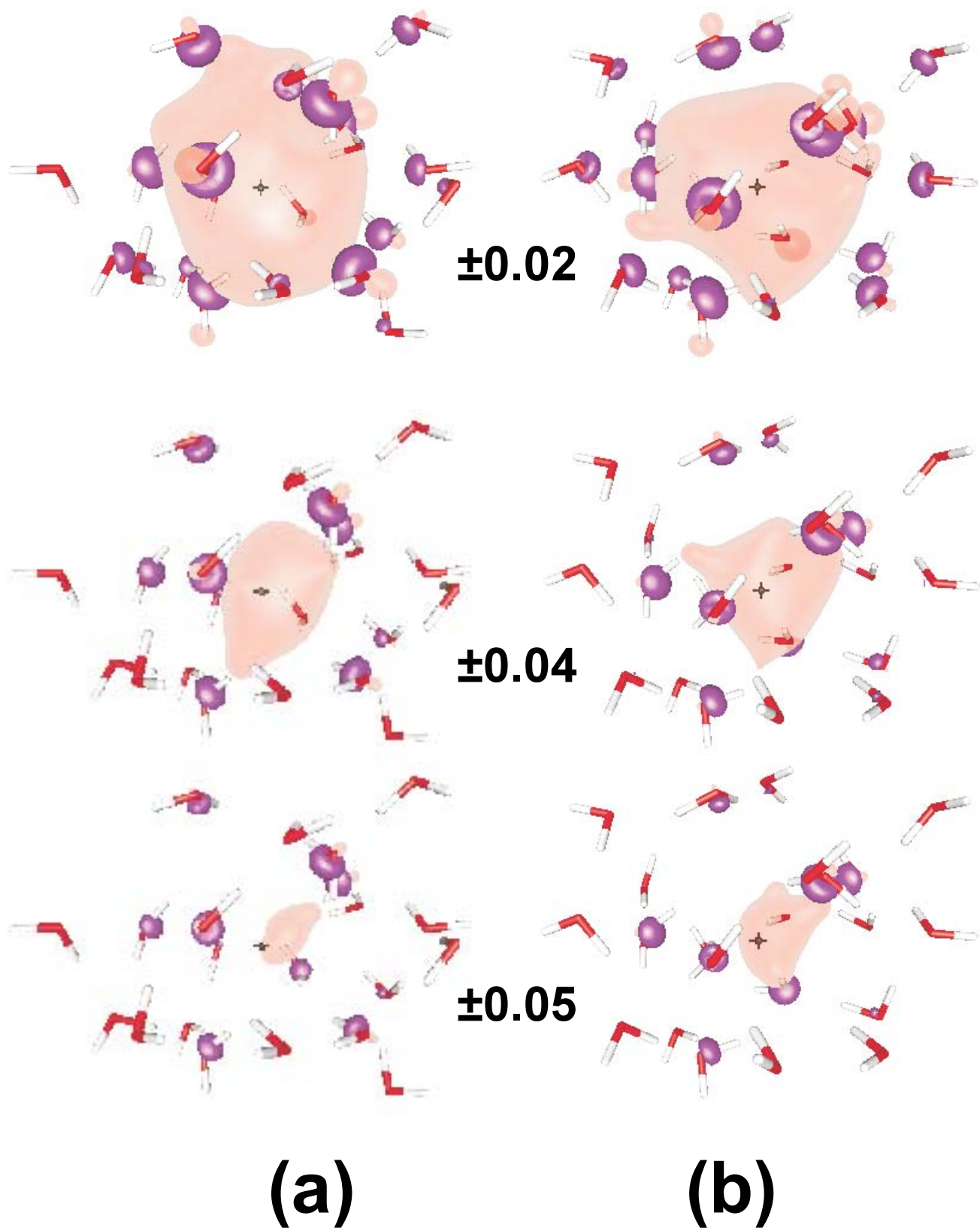


Figure 3S; Shkrob et al.

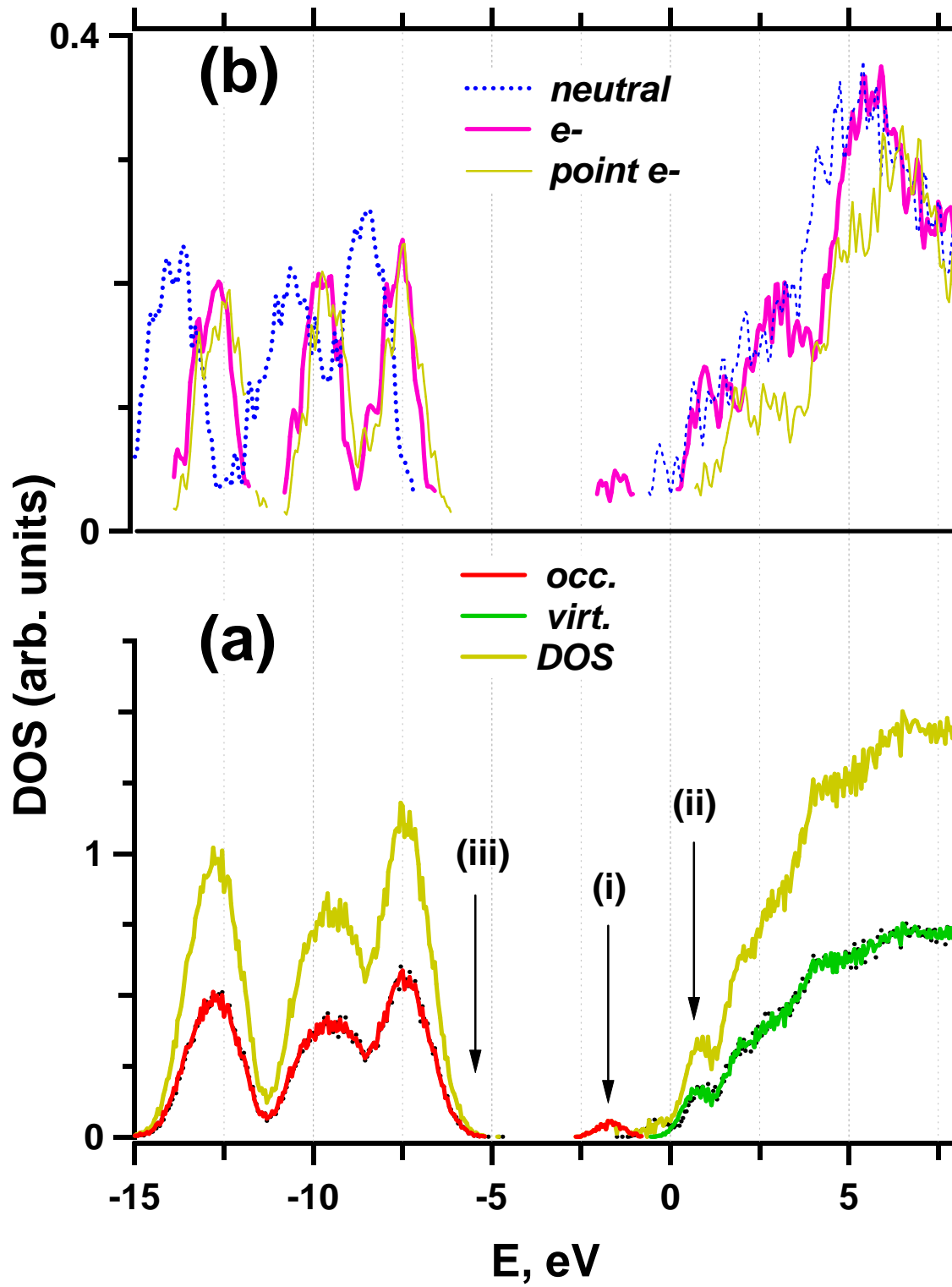


Figure 4S; Shkrob et al.

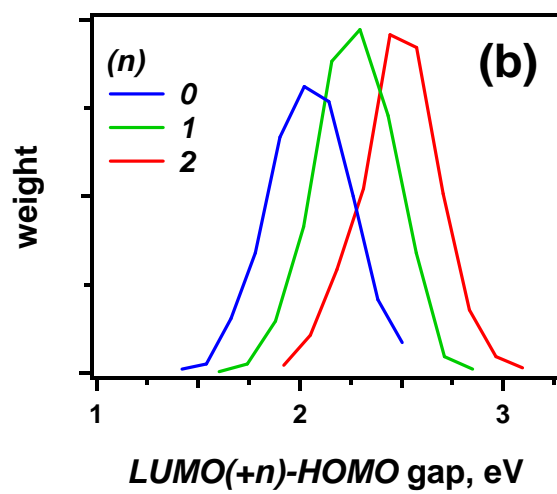
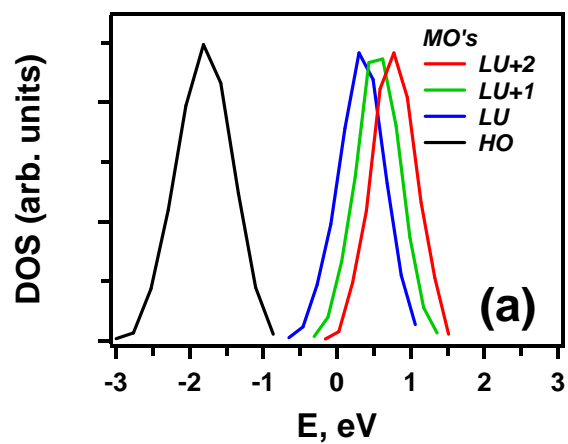


Figure 5S; Shkrob et al.

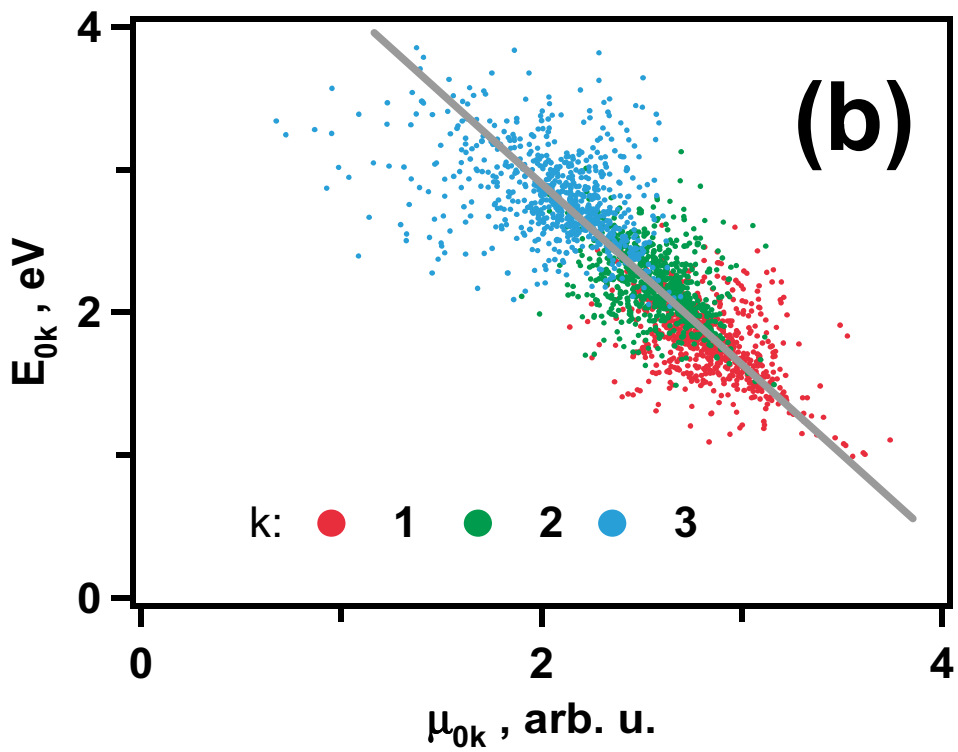
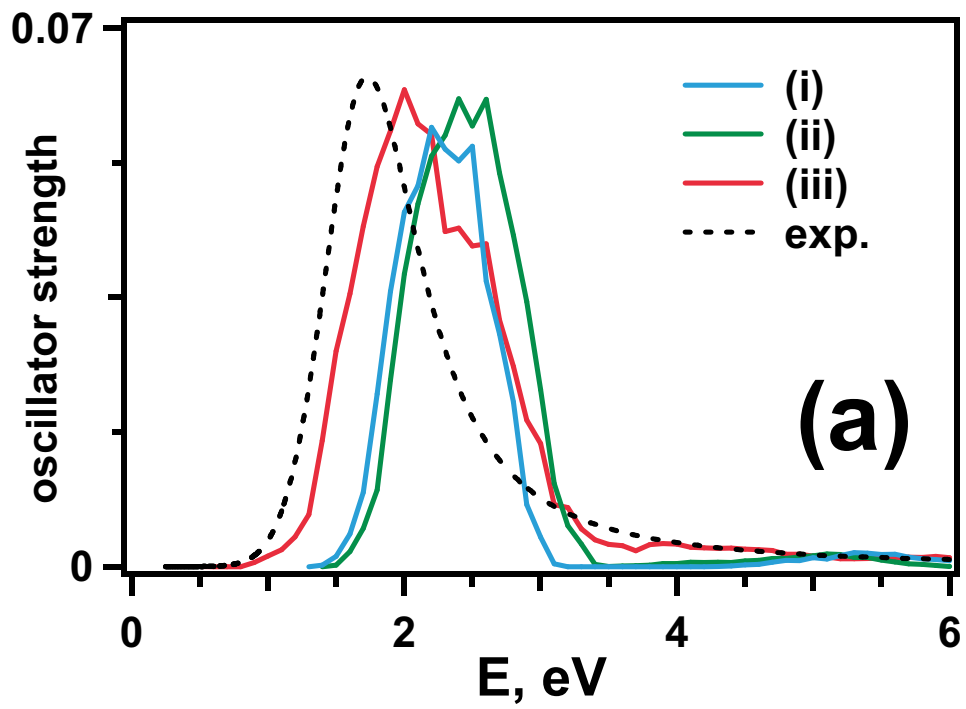
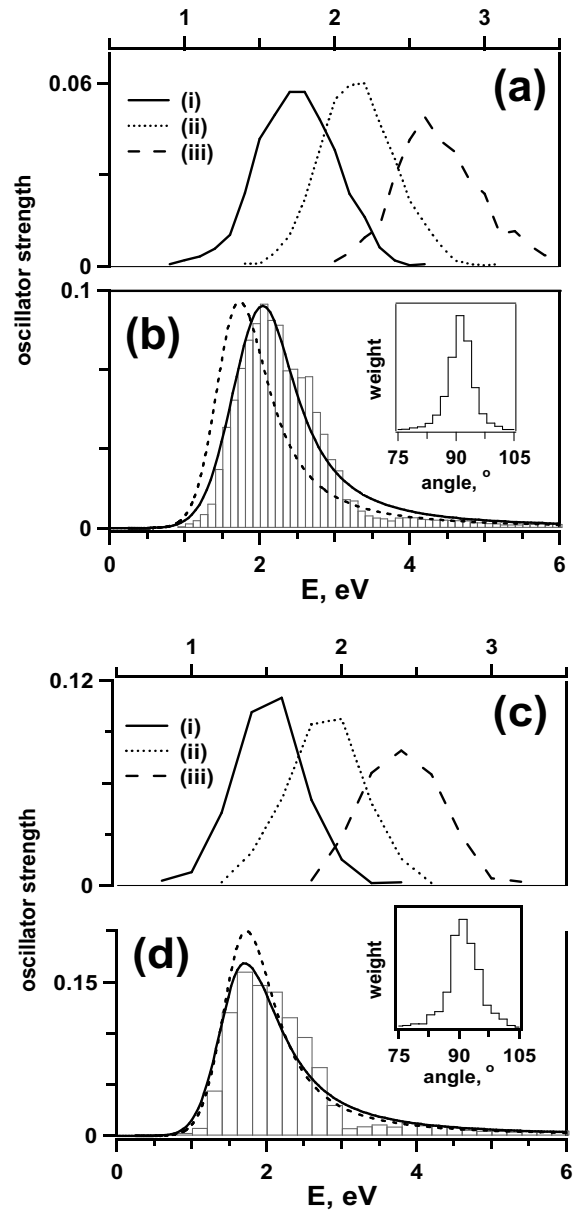
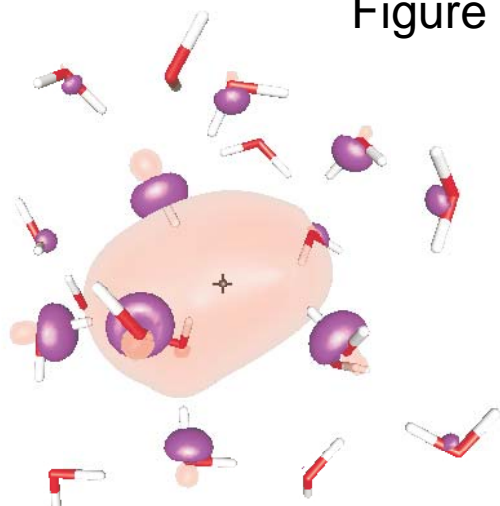


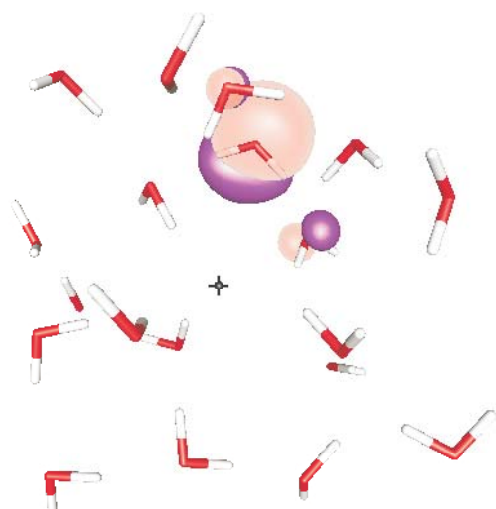
Figure 6S; Shkrob et al.



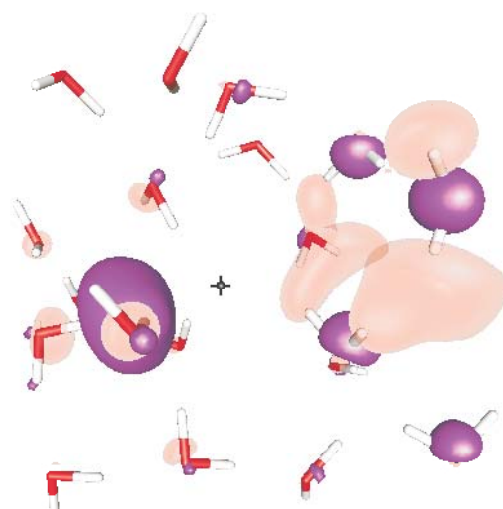
$\pm 0.03$



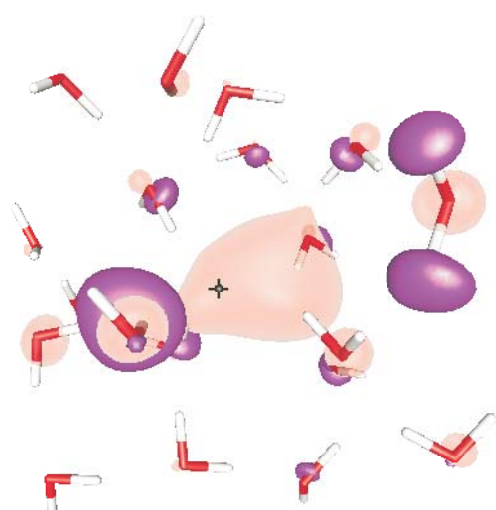
(a) HOMO



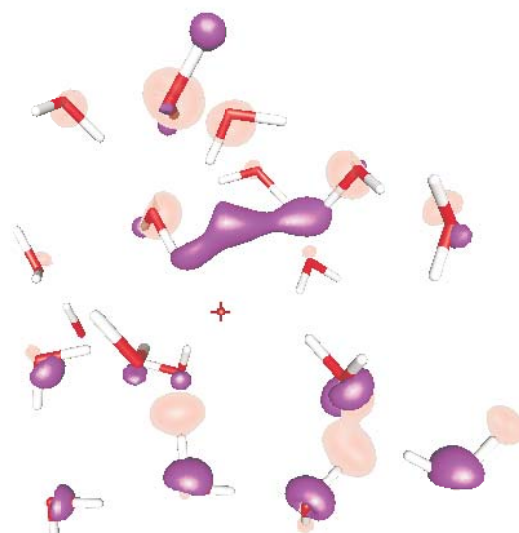
(b) HOMO-1



(c) LUMO

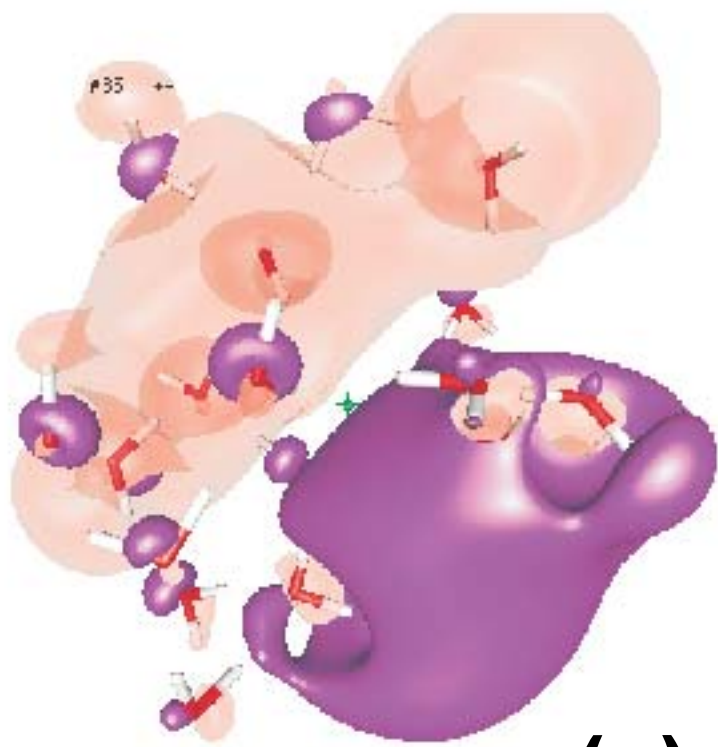


(d) LUMO+1

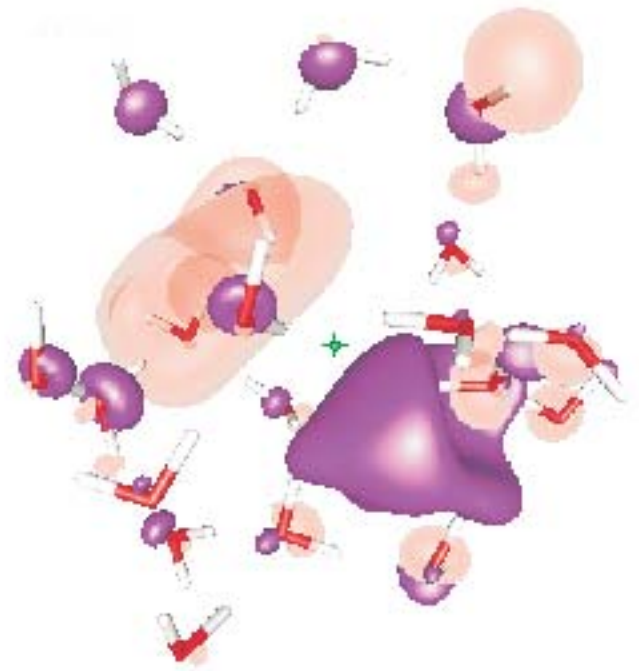


(e) LUMO+2

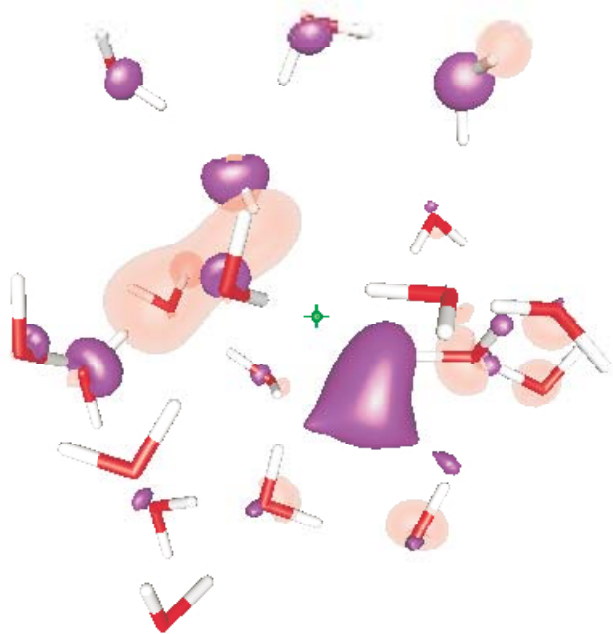
Figure 8S; Shkrob et al.



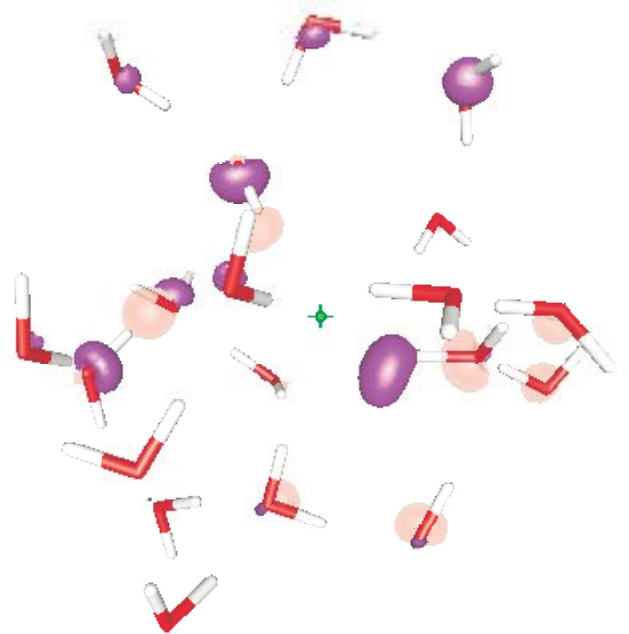
**(a)**



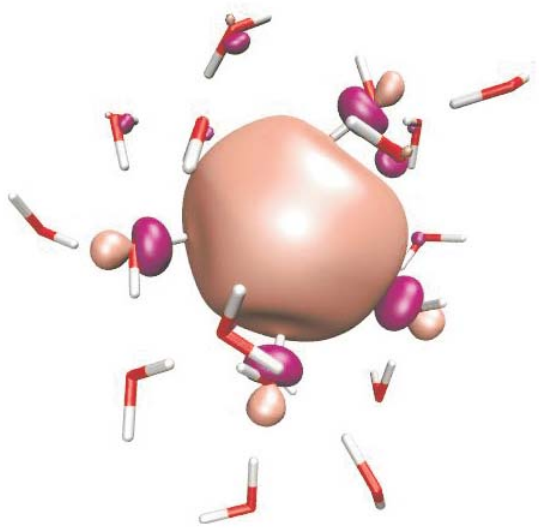
**(b)**



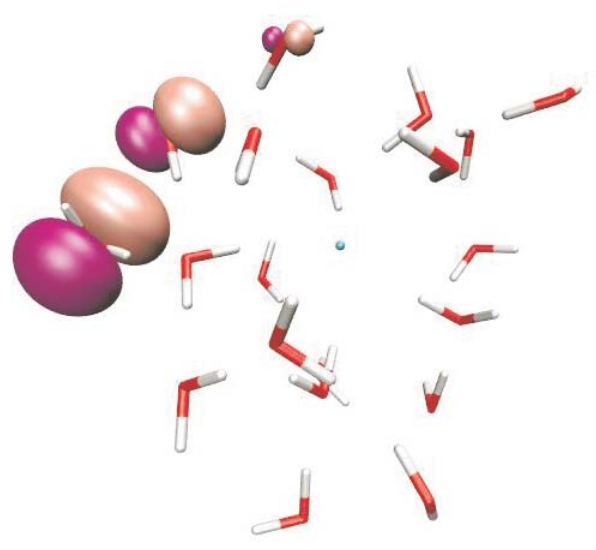
**(c)**



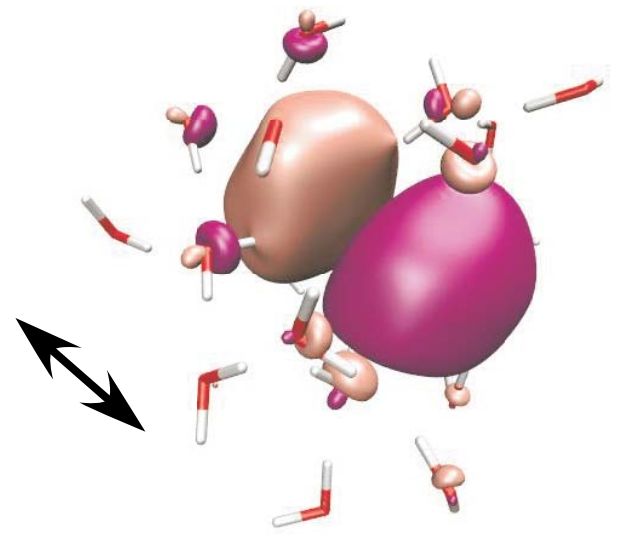
**(d)**



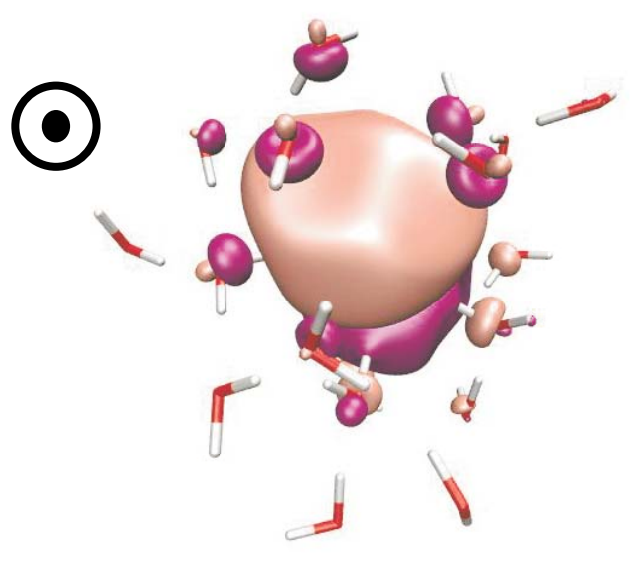
(a) HOMO



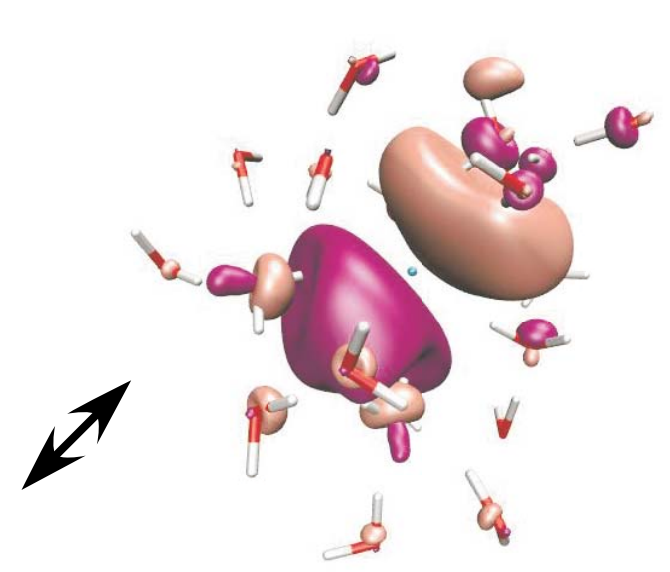
(b) HOMO-1



(c) LUMO



(d) LUMO+1



(e) LUMO+2

Figure 10S; Shkrob et al.

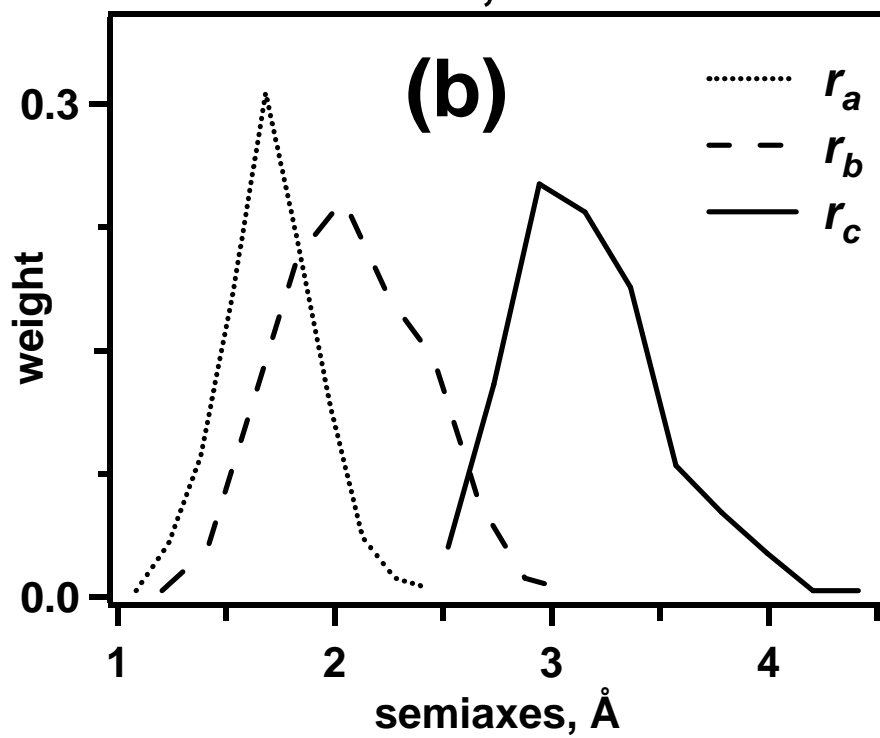
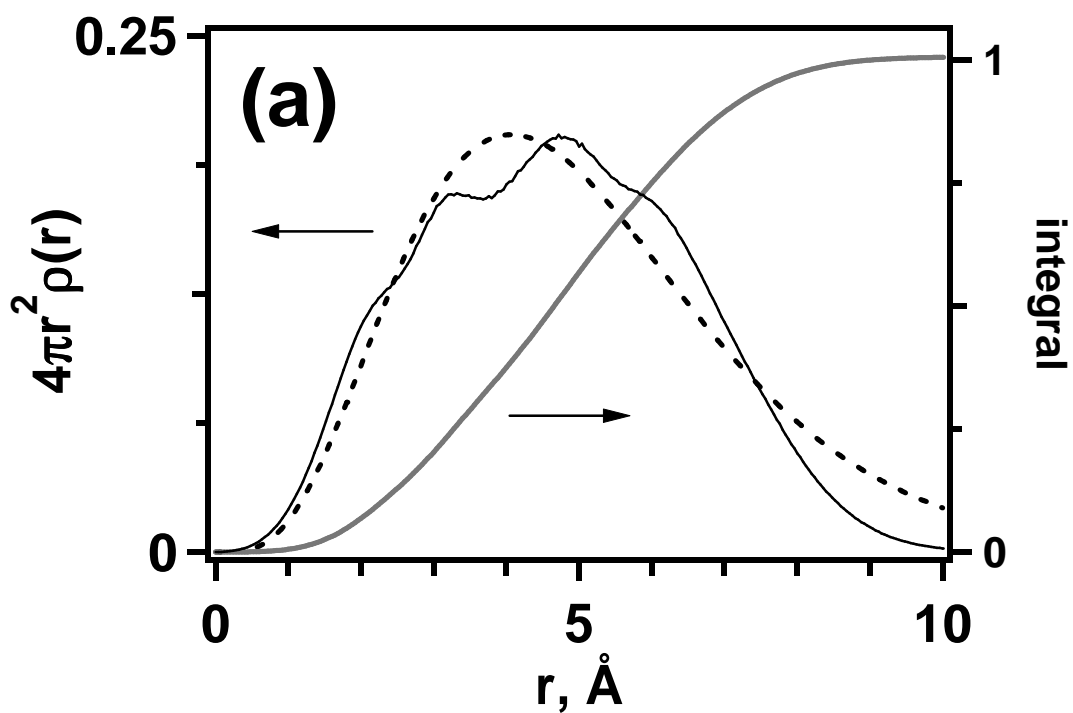


Figure 11S; Shkrob et al.

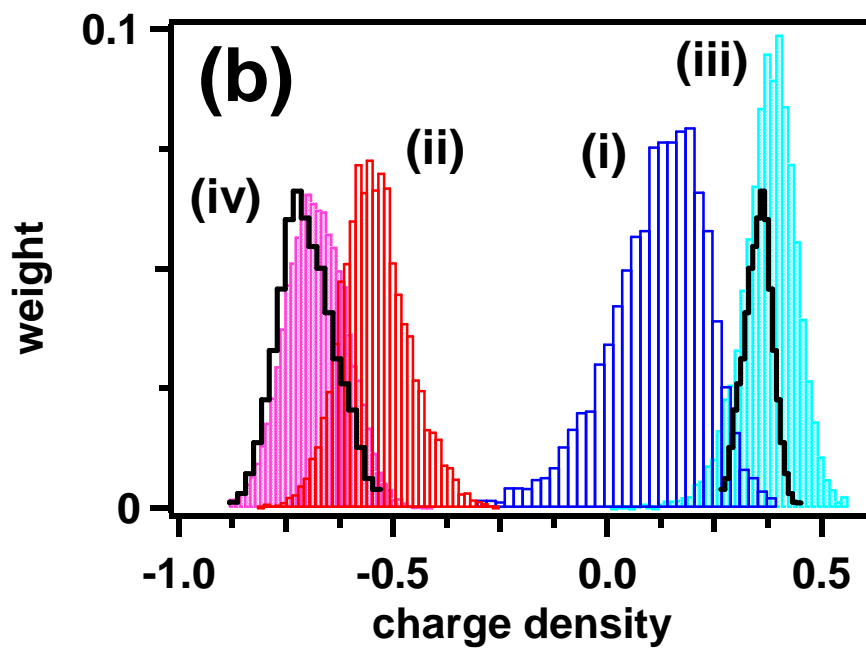
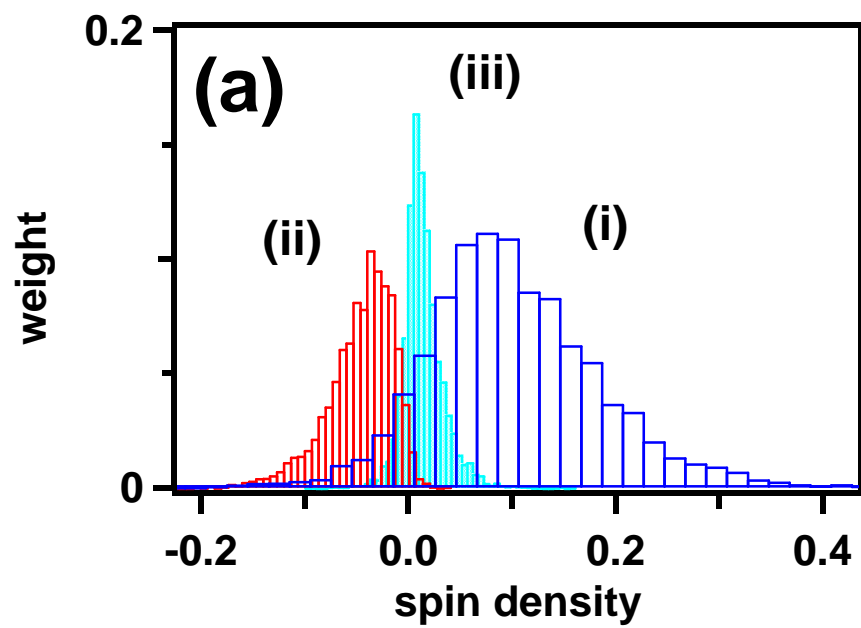


Figure 12S; Shkrob et al.

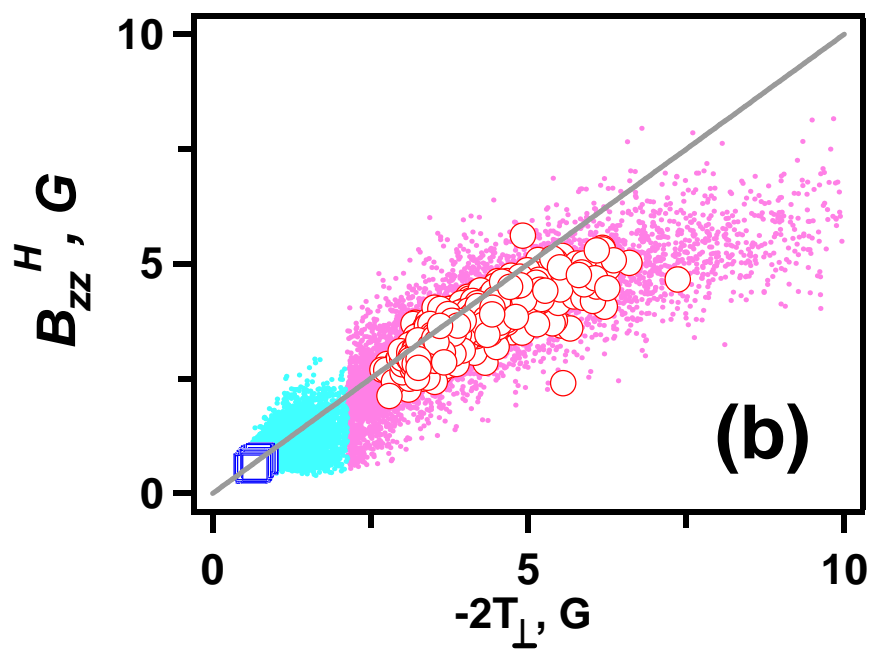
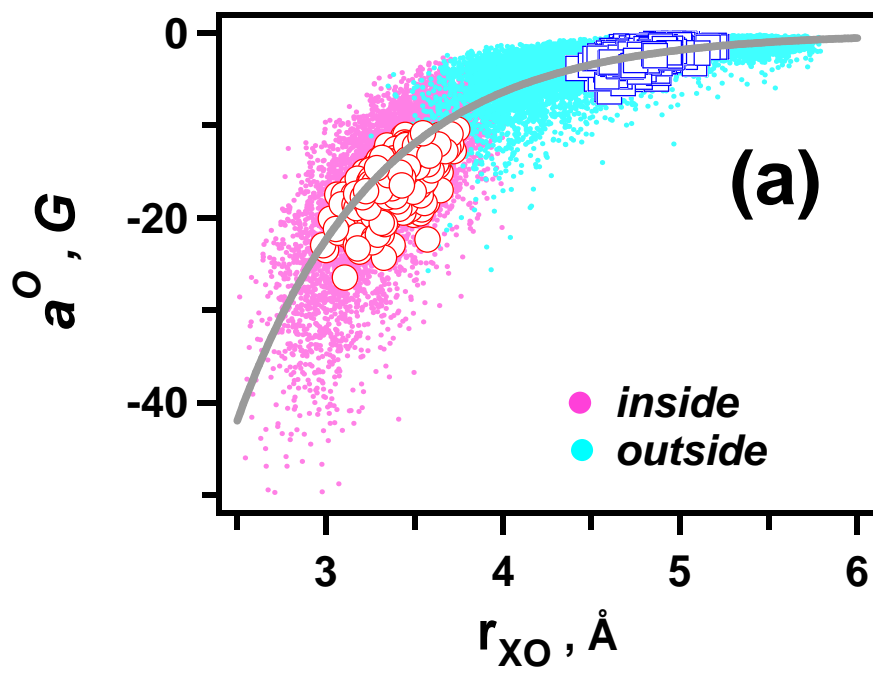


Figure 13S; Shkrob et al.

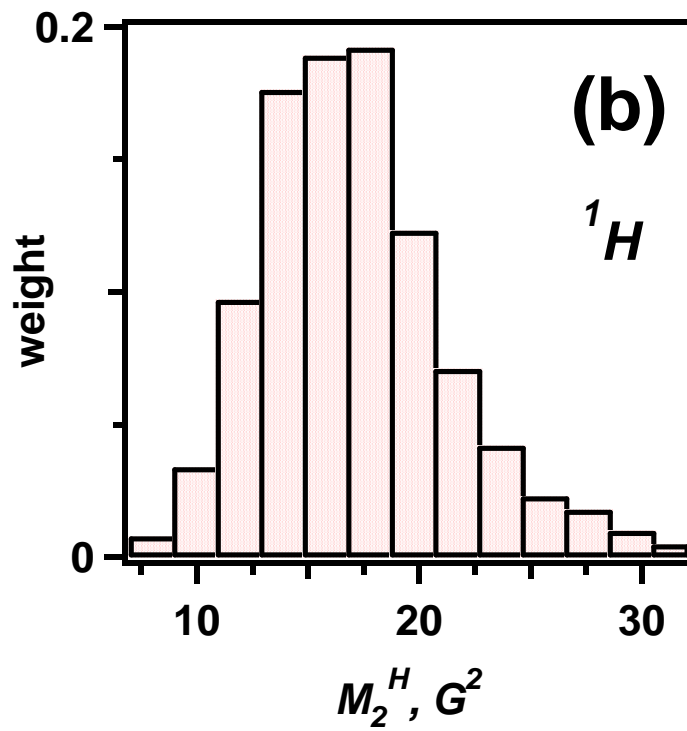
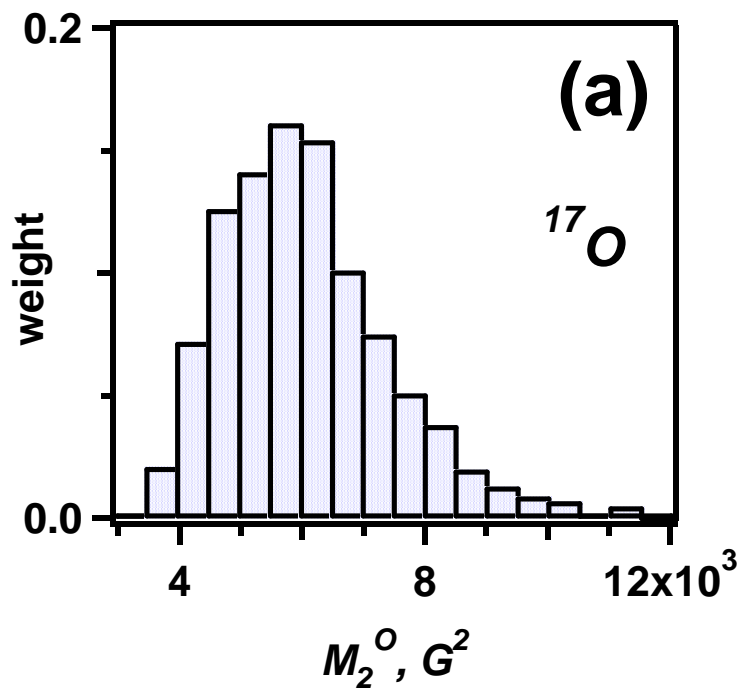


Figure 14S; Shkrob et al.

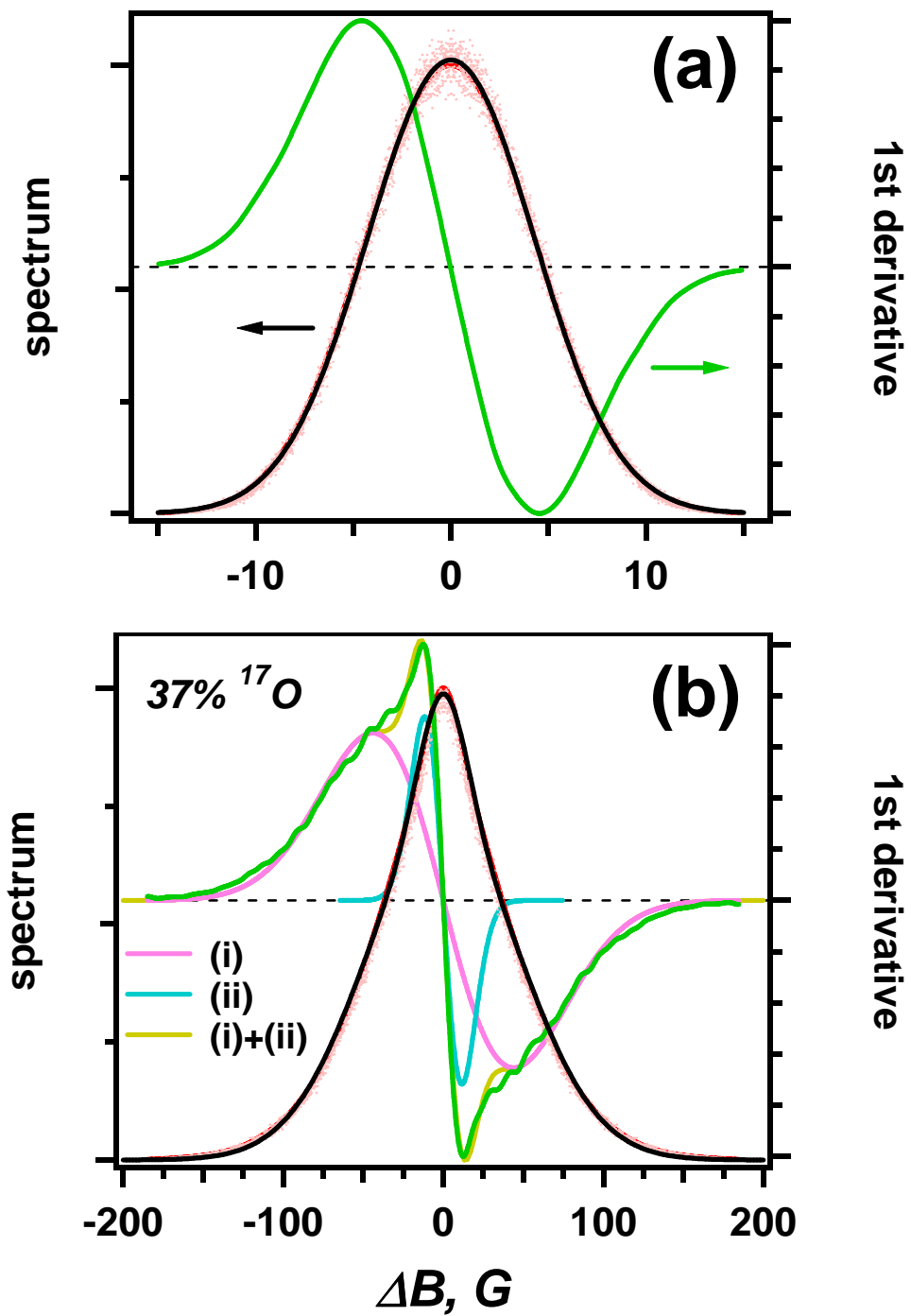


Figure 15S; Shkrob et al.

